Microwave Engineering
Ulm University

ulm university universität
uulm

High Range and Doppler Resolution by Application of Compressed Sensing Using Low Baseband Bandwidth OFDM Radar

Christina Knill, Benedikt Schweizer, Susanne Sparrer, Fabian Roos,
Robert F. H. Fischer, and Christian Waldschmidt

DOI: 10.1109/TMTT.2018.2830389

High Range and Doppler Resolution by Application of Compressed Sensing Using Low Baseband Bandwidth OFDM Radar

Christina Knill, Benedikt Schweizer, *Student Member, IEEE,* Susanne Sparrer, Fabian Roos, *Student Member, IEEE,* Robert F.H. Fischer, *Senior Member, IEEE,* and Christian Waldschmidt, *Senior Member, IEEE*

***Abstract*—Multi-carrier waveforms such as orthogonal frequency-division multiplexing (OFDM) found their way into radar applications in the last few years. However, currently, typically only a fraction of the large baseband bandwidth required to obtain high resolution is available in practice due to hardware limitations. In this paper, we propose a frequency agile sparse OFDM radar processing which allows the transmission of consecutive bandwidth-reduced OFDM pulses on different carriers and thereby covering a much larger measurement bandwidth in a measurement frame. Through joint processing of multiple narrowband pulses and compressed sensing methods, high resolution and unambiguity in the joint range-velocity profile is obtained comparable to an equivalent wideband OFDM. It shows that a baseband bandwidth of 20 % of the full channel bandwidth is sufficient to reliably obtain the same result as for an equivalent wideband OFDM signal. The proposed processing scheme is validated using simulations and radar measurements at 77 GHz.**

***Index Terms*—approximate message passing, automotive radar, compressed sensing, OFDM, sparse signal processing, sub-nyquist sampling**

I. Introduction

ORTHOGONAL frequency-division multiplexing (OFDM) is widely used in communication systems, especially in wireless communications, due to its flexibility, robustness to narrowband channel fading, high throughput, and its applicability as a frequency-division multiple access (FDMA) scheme [1]. The application of OFDM in radar sensing was first proposed by Levanon [2]. Driven by the idea to combine radar and communication [3]–[5], various signal processing improvements for radar applications were presented since then. The exact matched filter for OFDM radar is derived in [6]. In [7], [8], radar image processing based on the Fourier transform to gain joint range and velocity information is applied, similar to chirp-sequence processing. Since most of the signal processing is done digitally, pure OFDM radar enables new possibilities for flexible and adaptive radar schemes. However, in contrast to FMCW radar, OFDM radar has the drawback that the baseband and RF bandwidth are identical. Furthermore, the achievable resolution in range is proportional to the reciprocal of the RF bandwidth. Hence, to achieve high range resolution, a large RF and, consequently, baseband bandwidth is required. This also means that the wideband signal has to be AD/DA converted at the transmitter and receiver. Especially in automotive applications, high-resolution as well as large unambiguity regions for range and velocity are required. For example, a resolution of $10\,\mathrm{cm}$ requires a bandwidth of $1.5\,\mathrm{GHz}$. It is foreseeable that a hardware offering sufficient high sampling and data processing rates will not be achievable in near future.

Hence, various suggestions to reduce the required OFDM bandwidth, and thereby the hardware requirements, have been proposed recently. A promising idea is to combine narrowband OFDM signals and frequency agility, in terms of subsequent transmission on different carriers.

In [9], a frequency-hopping OFDM concept is presented. High range resolution is achieved by synthesizing multiple narrowband signals of different carriers. This method is only for stationary or low-velocity targets. In [10], a similar frequency-agile concept is presented where also Doppler processing is investigated. Different frequency-agility strategies, narrowband and wideband, are proposed and evaluated. In [11], OFDM processing to achieve high-resolution in range is shown using linearly increasing discrete frequency steps. Again, the method is only applicable for small velocities. A processing scheme seeking both high range and velocity resolution using linear repetitive frequency steps is proposed in [12]. The processing of the receive signal is achieved using the fast Fourier transform (FFT). Due to the constant step repetition, the unambiguous Doppler range is reduced compared to the equivalent full OFDM transmission by the number of steps.

A drawback of many of these deterministic low-bandwidth, frequency-agile OFDM concepts is that they lack Doppler processing concepts and flexibility compared to an equivalent wideband OFDM. Moreover, high resolution is achieved at the expense of unambiguity. To overcome these limitations, we propose a flexible, non-deterministic processing concept combining low-bandwidth signals, random frequency-hopping, and compressed sensing methods. In the following, this concept is referred to as *sparse OFDM*.

Compressed Sensing (CS) [13], [14] is a powerful tool to estimate or reconstruct a high-dimensional signal from its sub-

Manuscript received December 6, 2017; The research leading to these results was conducted within the Tech Center a-drive and was funded by the MWK Baden-Württemberg (32-7533-4-10/13/20). Responsibility for the information and views set out in this publication lies entirely with the authors.

C. Knill, B. Schweizer, F. Roos, and C. Waldschmidt are with the Institute of Microwave Engineering, Ulm University, 89081 Ulm, Germany (e-mail: christina.knill@uni-ulm.de).

S. Sparrer, and R.F.H. Fischer are with the Institute of Communications Engineering, Ulm University, 89081 Ulm, Germany.

Nyquist sampled low-dimensional and noisy observations. In OFDM radar applications, CS is applied to improve passive radar detection [6], [15]. In [16], CS is used for interference mitigation in a combined communication and radar system. A sub-Nyquist OFDM radar system is presented in [17]. A set of bandpass filters are used to sample portions of a wideband OFDM signal block-wisely. The signal is reconstructed using CS methods. Additionally, an optimal sampling strategy is proposed. In [18], a high range resolution (HRR) radar based on the frequency-agile concept in [9] is shown. The reconstruction of signals using regularly subsampled or decimated measurement matrices is addressed. However, the method does not address Doppler processing.

In this paper, we propose a concept that combines CS and narrowband OFDM and offers the possibility to preserve resolution and unambiguity of a wideband OFDM signal but requiring only a fraction of its baseband bandwidth. Furthermore, joint range-velocity processing to gain information of targets via straightforward FFT is possible similar to the standard OFDM radar. To increase the aimed measurement bandwidth, the wider RF bandwidth is achieved by subsequent transmission of narrowband OFDM signals using different carrier frequencies, similar to frequency-hopping. The meaning of narrowband in this context means narrow compared to the aimed large channel bandwidth. Instead of linear and periodical frequency concepts, which reduce the Doppler unambiguity due to periodic subsampling of the signal, discrete but randomly chosen frequencies are used in order to preserve the unambiguity of the original equivalent full OFDM and enable CS processing to reconstruct the noisy, sub-Nyquist sampled signal. Furthermore, the scheme allows using altering bandwidths and lengths of the consecutive narrowband signals.

We show that applying CS to a sparse OFDM signal, consisting of synthesized narrowband OFDM blocks, allows reconstruction of the radar scene exhibiting the same resolution as with an equivalent full OFDM radar without loss of unambiguity. Additionally, due to the significant reduction of the signal bandwidth in sparse OFDM, the requirement on AD/DA converters, mixers, amplifiers, filters, data throughput, and storage are relaxed. It turns out, that, with the proposed sparse OFDM processing scheme, only 10% to 30% of the total measurement bandwidth is required to obtain a comparable result as with an equivalent full-bandwidth OFDM signal regarding resolution and unambiguity of range and Doppler.

The paper is organized as follows. In Section II, a short introduction to standard full OFDM is given. Signal generation, receive processing, and evaluation of sparse OFDM signals without CS is presented in Section III. In Section IV, a short introduction to CS and the applied algorithms and methods are presented. In Sections V and VI, the processing scheme is validated using simulations and radar measurements of extended targets.

II. Standard OFDM Radar

In this section, required properties of an OFDM radar signal are briefly summarized. An idealized OFDM signal is composed of $\mathcal{N}$ orthogonal continuous wave (CW) signals, usually referred to as subcarriers. On every subcarrier, a random sequence of data symbols is transmitted. Assuming the duration of each symbol to be T, the frequency spacing of the subcarriers to guarantee orthogonality is $\Delta f = 1/T$. Hence, the resulting signal bandwidth is $\mathcal{W}{=}\mathcal{N}\Delta f$.

An idealized OFDM symbol is given by

$$x(t) = \sum_{\nu=0}^{\mathcal{N}-1} d(\nu)\mathrm{e}^{\mathrm{j}2\pi\nu\Delta f t}\mathrm{rect}\left(\frac{t}{T}\right), \tag{1}$$

where $d(\nu)$ is the complex data symbol on the ν^{th} subcarrier which is drawn from a finite set (signal constellation, here we assume QPSK). A sequence of $\mathcal{M}$ individual OFDM symbols is called a frame. This scheme is further referred to as full OFDM.

In practice, this theoretic signal (1) is approximated via discrete-time processing. To this end, the block of data symbols $\boldsymbol{d} = [d(0), \ldots, d(\mathcal{N}-1)]$ is fed to an inverse discrete Fourier transform (IDFT). To handle the intersymbol interference (ISI) due to signal delays caused by targets in the channel, a cyclic prefix (CP) of $N_{\mathrm{cp}}{=}\mathcal{N}T_{\mathrm{cp}}/T$ samples is added. The discrete-time sequence is then DA-converted and filtered in order to suppress spectral replica. Finally, the baseband signal is mixed to a carrier frequency, and transmitted. Noteworthy, the digitally generated, practical OFDM signal is never identical to (1) since alias components due to the periodic nature of the spectrum of discrete-time signals cannot be removed via the filtering of the DA-converted signal.

To simplify the exposition and emphasize the theoretical concepts, the idealized OFDM signal is treated in the following and the CP is neglected.

III. Sparse OFDM

The range resolution of an OFDM radar is given by

$$\Delta R = \frac{c_0}{2\mathcal{W}} \tag{2}$$

with c_0 the speed of light. Using typical state-of-the-art industrial or automotive radars sensors to sample and process the aimed large RF bandwidth required for high resolution is impractical, even unrealizable in near future.

To overcome the bandwidth limitations due to hardware restrictions, we combine a smaller available bandwidth and frequency-agility to obtain a larger measurement bandwidth. The frequency-hopping can be realized with a variation of the monofrequent local oscillator (LO) signal. This signal is used for both up- and down-conversion, hence, the absolute phase of the LO signal does not matter. To cover a large bandwidth, the LO must be able to perform fast frequency-hopping within the range of the desired measurement bandwidth. Enhancing the processing concepts of [12] and [19], instead of equal-sized OFDM pulses or a strict periodic frequency pattern, we use short sequences of narrowband OFDM pulses of different bandwidths and a randomly chosen discrete frequency pattern. This has the advantage that periodic subsampling is avoided and the resulting significant loss in Doppler unambiguity is prevented such that the unambiguity of the full transmission is available.

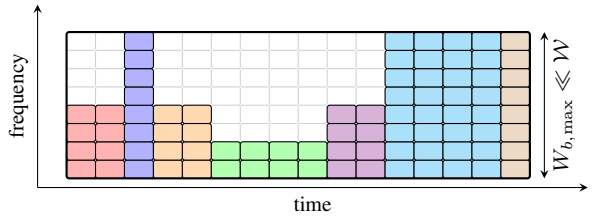

Fig. 1. Sparse OFDM baseband signal in time-frequency representation using seven blocks of different bandwidths and durations. Each filled box corresponds to an occupied symbol and white boxes indicate blank elements.

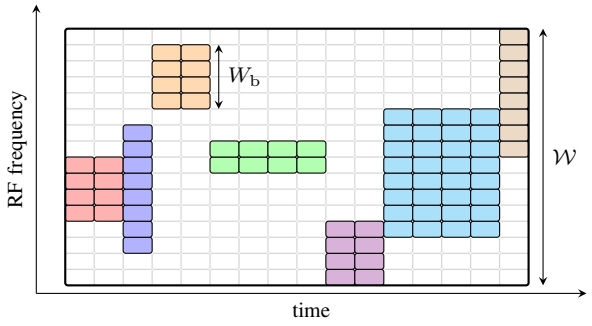

Fig. 2. Sparse OFDM signal in RF time-frequency domain of the low-baseband signal shown in Fig. 1. The sparse OFDM signal covers the same total duration and measurement bandwidth as a comparative full OFDM.

A. Transmit Signal Representation and Generation

In one measurement frame, B individual subsequent short narrowband OFDM signals, each consisting of M_b OFDM symbols and N_b subcarriers, $b = 0, \dots, B-1$, are transmitted. In the following, such signals are simply referred to as blocks. In Fig. 1, a baseband time-frequency representation of seven consecutive blocks is shown exemplary. With $d_b(m,n)$ representing the m^{th} QPSK symbol of length T, transmitted on the n^{th} subcarrier of the b^{th} block, the baseband signal of one block is then described by

$$x_b(t) = \sum_{m=0}^{M_b-1} \sum_{n=0}^{N_b-1} d_b(m,n) \mathrm{e}^{\mathrm{j}2\pi n \Delta f t} \mathrm{rect}\left(\tfrac{t-mT}{T}\right). \quad (3)$$

Before transmission, the OFDM symbols of each block are mixed to their common block carrier f_b. In order to preserve orthogonality among all subcarriers throughout the measurement frame, i.e., multiple blocks, only discrete carrier frequencies on the grid of $f_c + k\Delta f$, $k \in \mathbb{N}_0$, are allowed. Thereby, f_c is the lowest possible carrier which corresponds to the carrier frequency of full OFDM. Additionally, the signal may not exceed the allowed usable RF bandwidth $\mathcal{W}$ at no time, limiting the maximum carrier frequency of an OFDM symbol with bandwidth W_b to

$$f_{b,\max} = f_c + \mathcal{W} - W_b = f_c + (\mathcal{N} - N_b)\Delta f. \quad (4)$$

Hence, the individual block carrier frequency is

$$f_b = f_c + k_b \Delta f \quad \text{with} \quad k_b \in \{0, 1, \dots, (\mathcal{N} - N_b)\}, \quad (5)$$

where $\boldsymbol{k} = [k_0, k_1, \dots, k_{B-1}]$ indicates the frequency-hopping pattern.

Using (5), the resulting RF signal of (3) after up-conversion is

$$x_b^{\mathrm{RF}}(t) = \sum_{m=0}^{M_b-1} \sum_{n=0}^{N_b-1} d_b(m,n) \mathrm{e}^{\mathrm{j}2\pi((n+k_b)\Delta f + f_c)t} \mathrm{rect}\left(\tfrac{t-mT}{T}\right). \quad (6)$$

For example, the resulting RF transmit signal of the baseband signal depicted in Fig. 1 leads to a patchwork-like structure as shown in Fig. 2.

Compared to full OFDM, only a fraction $\gamma \in [0,1]$ of the maximum baseband bandwidth

$$W_{b,\max} = N_{b,\max}\Delta f = \gamma \mathcal{W} \quad \Rightarrow \quad \gamma \approx \frac{W_{b,\max}}{\mathcal{W}}$$

is used with $N_{b,\max}$ and $W_{b,\max}$ the number of subcarriers and bandwidth of the widest block, respectively. Instead of $\mathcal{M}\mathcal{N}$ symbols per frame in full OFDM, only $\gamma\mathcal{M}\mathcal{N}$ are required in sparse OFDM. This reduces the required amplifier, mixer, filter, and AD/DA bandwidth and the sampling rate by a factor γ.

B. Transmission Pattern

In the RF band, the sequence of B transmitted blocks of a measurement frame covers the same measurement bandwidth and time as the equivalent full OFDM signal. In the following example, different from Fig. 2, non-partially overlapping (in frequency) blocks are used for simpler description. Using matrix representation, a frame with seven blocks $\boldsymbol{x}_b \in \mathbb{R}^{N_b \times M_b}$, yields in time-frequency domain

$$\boldsymbol{X} = \begin{bmatrix} \mathbf{0} & \mathbf{0} & \mathbf{0} & \mathbf{0} & \boldsymbol{x}_4 & \mathbf{0} & \mathbf{0} \\ \mathbf{0} & \boldsymbol{x}_1 & \mathbf{0} & \boldsymbol{x}_3 & \mathbf{0} & \mathbf{0} & \mathbf{0} \\ \boldsymbol{x}_0 & \mathbf{0} & \mathbf{0} & \mathbf{0} & \mathbf{0} & \boldsymbol{x}_5 & \mathbf{0} \\ \mathbf{0} & \mathbf{0} & \boldsymbol{x}_2 & \mathbf{0} & \mathbf{0} & \mathbf{0} & \boldsymbol{x}_6 \end{bmatrix} \quad (7)$$

with $\boldsymbol{X} \in \mathbb{R}^{\mathcal{N} \times \mathcal{M}}$. Replacing the block matrices $\boldsymbol{x}_b$ by all-ones matrices $\mathbf{1}$ of the same size, the so-called transmission pattern

$$\boldsymbol{P} = \begin{bmatrix} \mathbf{0} & \mathbf{0} & \mathbf{0} & \mathbf{0} & \mathbf{1} & \mathbf{0} & \mathbf{0} \\ \mathbf{0} & \mathbf{1} & \mathbf{0} & \mathbf{1} & \mathbf{0} & \mathbf{0} & \mathbf{0} \\ \mathbf{1} & \mathbf{0} & \mathbf{0} & \mathbf{0} & \mathbf{0} & \mathbf{1} & \mathbf{0} \\ \mathbf{0} & \mathbf{0} & \mathbf{1} & \mathbf{0} & \mathbf{0} & \mathbf{0} & \mathbf{1} \end{bmatrix} \quad (8)$$

is obtained. The pattern matrix contains only zeros and ones where zeros indicate unused and ones indicate used blocks of subcarriers and symbols.

C. Receive Signal

At the receiver, the OFDM symbols of each block are down-converted to the baseband using their individual transmit carrier frequencies f_b provided by the same oscillator as for up-conversion.

Assuming a simple point scatterer model, a signal reflected from a target h is an attenuated and delayed version of the transmitted signal. The delay is given by

$$\tau_h = \frac{2r_h(t)}{c_0} = \frac{2(r_{0,h} - v_h t)}{c_0} \quad (9)$$

with range progression $r_h(t)$, relative velocity v_h, and initial range $r_{0,h}$ of the target.

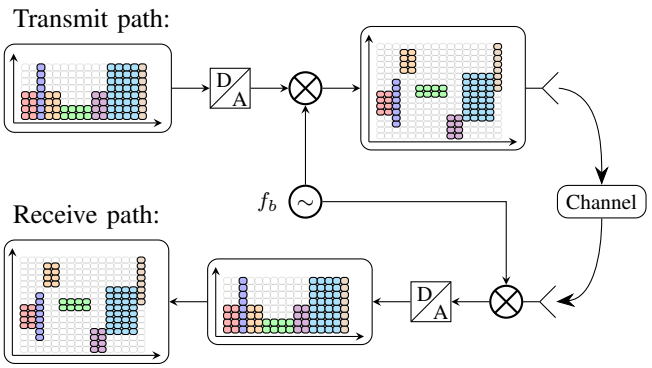

Fig. 3. Abstraction of the signal flow of transmit and receive path.

Neglecting attenuation due to reflection as well as free-space losses and multipath propagation, the baseband receive signal of (3) reflected by a single target is

$$\begin{aligned} y_b(t) &= \sum_{m=0}^{M_b-1}\sum_{n=0}^{N_b-1} d_b(m,n)\mathrm{e}^{-\mathrm{j}2\pi(n\Delta f+f_b)\tau}\mathrm{e}^{\mathrm{j}2\pi n\Delta f t} \\ &= \sum_{m=0}^{M_b-1}\sum_{n=0}^{N_b-1} d'_b(m,n)\mathrm{e}^{\mathrm{j}2\pi n\Delta f t} \end{aligned} \tag{10}$$

where the first and third term are part of the transmit signal in (3) and the second term is target dependent. The term $d'_b(m,n)$ contains the QPSK symbols $d_b(m,n)$ altered by the channel and hence constitute the received symbols.

Next, each OFDM symbol is sampled using the sampling frequency

$$f_{s,\max} = 2N_{\max}\Delta f = \gamma f_{s,\text{full}} \tag{11}$$

limited by the widest block. This sampling frequency is only a factor γ of the Nyquist frequency $f_{s,\text{full}}$ of the equivalent full OFDM.

Afterwards, an FFT over every OFDM symbol of the block is performed to obtain the information of the subcarriers. In the last step, the modulating terms $d_b(m,n)$ are removed from the received symbols $d'_b(m,n)$ in (10) which gives the pure action of the channel in frequency domain. Plugging in (9) and replacing t by mT yields

$$\begin{aligned} D_b(m,n) &= \frac{d'_b(m,n)}{d_b(m,n)} \\ &= \mathrm{e}^{-\mathrm{j}2\pi\left(\frac{2r_0}{c_0}(f_b+n\Delta f)\right)}\mathrm{e}^{\mathrm{j}2\pi\left(\frac{2v(m+\Sigma_M)T}{c_0}(f_b+n\Delta f)\right)} \end{aligned} \tag{12}$$

with Σ_M the number of preceding symbols in the measurement frame. The receive frame comprising M_b OFDM symbols and N_b frequency bins is given by

$$\boldsymbol{D}_b = \Big[D_b(m,n)\Big]\Big|_{\substack{m=0,\dots,M_b-1\\ n=0,\dots,N_b-1}}^{M_b\times N_b} \tag{13}$$

in matrix representation.

D. Processing Scheme

Evaluation of range and Doppler using a single block $\boldsymbol{D}_b$ would result in low resolution not suitable for high-resolution automotive applications. To regain a wider total bandwidth, the baseband blocks have to be rearranged such that their phase relation is correct. A correct and unambiguous arrangement is derived through comparison of the matrices $\boldsymbol{D}_b$ with the equivalent full OFDM receive signal.

TABLE I
EQUIVALENT FULL OFDM CONFIGURATION

Block duration/Number of symbols	$\mathcal{M}$	2048
Block bandwidth/Number of subcarriers	$\mathcal{N}$	2048
Baseband bandwidth (GHz)	W	1.024
RF bandwidth (GHz)	$\mathcal{W}$	1.024
Subcarrier spacing (kHz)	Δf	500
Cyclic prefix duration (µs)	T_{cp}	0.4
Maximum range (m)	$r_{\max}$	60
Range resolution (m)	Δr	0.15
Maximum velocity (m/s)	$v_{\max}$	±50
Velocity resolution (m/s)	Δv	0.39

TABLE II
SPARSE OFDM CONFIGURATIONS

	Full OFDM	Variable or fixed block sizes			
M_b	2048	$1, 2, 4, \dots, 256$			
N_b	2048	128	256	512	1024
W_b (MHz)	1 024	63.5	127.5	255.5	511.5
Δr_b (m) (per block)	0.15	2.36	1.18	0.59	0.29

An equivalent wideband OFDM receive frame $\boldsymbol{Y}'$ comprises $\mathcal{N}$ frequency bins and $\mathcal{M}$ OFDM symbols indicated by $\mu = 0, \dots, \mathcal{M}-1$ and $\nu = 0, \dots, \mathcal{N}-1$ respectively. The $(\mu,\nu)^{\text{th}}$ element of the full OFDM frame yields

$$Y'(\mu,\nu) = \mathrm{e}^{-\mathrm{j}2\pi\left(\frac{2r_0}{c_0}(f_c+\nu\Delta f)\right)}\mathrm{e}^{\mathrm{j}2\pi\left(\frac{2v\mu T}{c_0}(f_c+\nu\Delta f)\right)}. \tag{14}$$

Using the block frequency (5) and variable substitution

$$\mu = m + \Sigma_M \quad \text{and} \quad \nu = n + k_b \tag{15}$$

for each element $D_b(m,n)$ in (12) a unique corresponding full OFDM element $Y'(\mu,\nu)$ in (14) is obtained.

Consequently, the m^{th} symbol of the b^{th} block in the measurement frame is the $(m+\Sigma_M)^{\text{th}}$ transmitted symbol in total. Similarly, the n^{th} subcarrier of the b^{th} block equals $(n\Delta f + f_b)$ in full OFDM. Using the block frequency (5), this can be reformulated with $f_c + (n+k_b)\Delta f$.

Hence, the correct arrangement of the individual blocks is equal to the transmit structure (7) and the pattern (8). Consequently, the sparse signal to evaluate is

$$\boldsymbol{Y} = \begin{bmatrix} \mathbf{0} & \mathbf{0} & \mathbf{0} & \mathbf{0} & \boldsymbol{D}_4 & \mathbf{0} \\ \mathbf{0} & \boldsymbol{D}_1 & \mathbf{0} & \boldsymbol{D}_3 & \mathbf{0} & \mathbf{0} \\ \boldsymbol{D}_0 & \mathbf{0} & \mathbf{0} & \mathbf{0} & \mathbf{0} & \boldsymbol{D}_5 \\ \mathbf{0} & \mathbf{0} & \boldsymbol{D}_2 & \mathbf{0} & \mathbf{0} & \mathbf{0} \end{bmatrix} \tag{16}$$

with submatrices given by the blocks $\boldsymbol{D}_b$. Blank spaces are temporarily filled with zeros for evaluation.

A schematic overview of the proposed signal flow of the transmit and receive path is shown in Fig. 3.

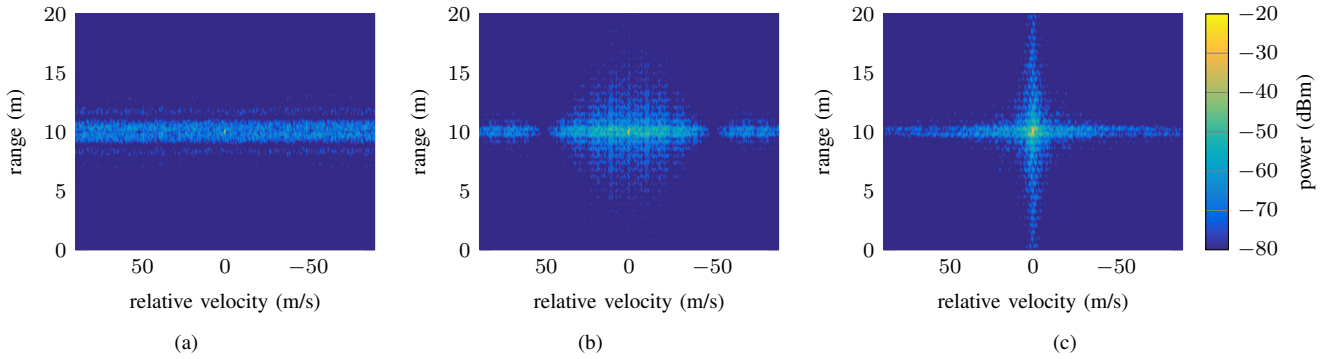

Fig. 4. Sparse OFDM radar images for different block configurations $N_b|M_b$: (a) $256|2$, (b) $512|16$, and (c) $512|2, \dots 256$.

E. Effects of the Signal Pattern on the Range-Doppler Evaluation

In conventional full OFDM radar, the radar image is obtained via IDFT (of each OFDM symbol) followed by a DFT processing (of each subcarrier) of the received signal frame. In [12], it is shown that this processing is also valid in case of empty signal elements. Furthermore, it is shown that the resulting radar image has the same resolution as full OFDM. However, due to the regular sub-sampling of the subcarriers, the unambiguous velocity is reduced by the number of frequency steps. Unlike in [12], the sampling period for a single subcarrier in sparse OFDM is not constant but random. As a consequence, the unambiguous velocity is not reduced compared to an equivalent full OFDM. Yet, as shown in [10], this improvement comes at the expense of rising artifacts in the range-velocity profile. At this point, it is worth mentioning that such a signal structure is not optimal for conventional FFT processing but is a basic prerequisite for subsequent compressed sensing methods, as will be detailed later on. In the following, the impact of the sparse signal structure on the radar image is examined.

An equivalent full OFDM signal bandwidth of approximate 1 GHz and an observation time of 5 ms is chosen. The corresponding full OFDM parameters are summarized in Table I. An excerpt of conceivable options of the narrowband OFDM blocks are listed in Table II. In sparse configuration, it is possible to keep either none, one, or both of M_b and N_b fixed to a specific value for all blocks or alter one or both of the parameters from block to block. The corresponding baseband bandwidth and range resolution for every block configuration is given in the table as well. A single target at distance of $r = 10\,\mathrm{m}$ with velocity $v = 0\,\mathrm{m/s}$ and radar cross-section (RCS) of $\sigma = 10\,\mathrm{m}^2$ is used.

In Fig. 4, the range-velocity profiles of three different sparse configurations are shown exemplary. Comparing the results, the characteristic ridge along the velocity at the target range is observable. In [10], it is shown that such a ridge emerges when narrowband blocks are transmitted at random frequencies. It is a result of the non-constant pulse repetition interval on every subcarrier. Demanding random block-transmission patterns in order to combat unambiguity loss, this effect is inevitable.

The extent of the ridge in range dimension is proportional to the bandwidth of the blocks, where a larger block bandwidth results in a thinner ridge as can be seen by comparing the ridges in Fig. 4a and Fig. 4b.

Another finding is that the extent of the ridge along v decreases when the block duration increases. The reason is that the ridge is actually the main lobe of a broad sinc-function proportional to the block duration.

If the block duration is chosen alternately and random (cf. Fig. 4c), an additional vertical ridge along r at the target velocity appears. The extent of this ridge is proportional to the maximum block duration. The longer the blocks are in average, the sharper this ridge gets.

In summary, compared to full OFDM, a sparse OFDM range-velocity profile exhibits artifacts due to the random transmission pattern structure. However, since it does not use a regular or periodic grid, it prevents unambiguity loss and enables the utilization of CS methods.

F. Alternative View

The same scheme is straightforwardly obtained starting from the desired wideband full OFDM signal transmitted at carrier f_c. If only a smaller bandwidth is measurable at once, symbols not located within the measurement band are irrelevant and can simply be set to zero. Thus, only N_b adjacent subcarriers within the measurement band are nonzero. For every OFDM symbol, the location of this band within the wideband OFDM symbol is chosen randomly. This results in a full OFDM transmit and receive signal representation equivalent to (7) and (10). The processing would be done as for standard OFDM, however, for all zero positions, no measurements are obtained.

Since all zero subcarriers are irrelevant, instead of f_c, the frequency of the lowest non-zero subcarrier, f_b, is sufficient for up- and down-conversion. Additionally, the bandwidth occupied by N_b adjacent subcarriers which has to be processed reduces to $N_b \Delta f$.

IV. Radar Image Reconstruction Using Compressed Sensing

In order to apply compressed sensing methods, besides the random property of the transmission pattern, the signal needs to be sparse in some transformation domain. The sparse nature of the introduced OFDM optimization problem arises from the finite number of targets present in the radar scene. Each

target has a distinct range and velocity mapped to an element in the range-velocity matrix. In this domain, only elements containing targets have an entry significant different from zero. Therefore, most radar signals are sparse in the joint range-velocity domain if the number of potential targets is much smaller than the range-velocity measurement space.

The conventional approach to the CS task is to solve the underdetermined system of equations given the observations $\boldsymbol{y} \in \mathbb{C}^{K\times 1}$ of an unknown signal $\boldsymbol{s} \in \mathbb{C}^{L\times 1}$, $K < L$,

$$\boldsymbol{y} = \boldsymbol{A}\boldsymbol{s} + \boldsymbol{n} \tag{17}$$

with $\boldsymbol{A} \in \mathbb{C}^{K\times L}$ and noise vector $\boldsymbol{n} \in \mathbb{C}^{K\times 1}$.

This approach is suitable for processing of arrays by exploiting their sparse structure in a transformation domain. For OFDM-radar applications, this is equal to reconstruction of either range or velocity dimension through row- or column-wise reconstruction of $\boldsymbol{Y}$ in (16). However, such a reconstruction of single OFDM symbols (rows) or subcarriers (columns) would not be able to cope with the dependence of its elements on both dimensions simultaneously. Thus, this dependency is not exploited in the reconstruction and further would result in poor range-velocity profiles and target detection. In order to gain performance by utilizing the intertwined information of range and velocity in $\boldsymbol{Y}$, the problem in (17) needs to be extended to matrices for the radar sensing case. The measurement vector $\boldsymbol{y}$ is converted to the matrix $\boldsymbol{Y}$. Likewise, the unknown vector $\boldsymbol{s}$ is converted to the unknown full OFDM range-velocity profile matrix. The matrix $\boldsymbol{A}$ is the link between the sub-Nyquist sampled time-frequency matrix $\boldsymbol{Y}$ and the range-velocity profile. It consists of DFT and IDFT processing of rows and columns, respectively, linking the information in time and frequency as well as the transmission pattern (8). A detailed description is given in Appendix A, for simplicity, we only use $\boldsymbol{A}$ in the following.

Using CS, our goal is to obtain a full measurement approximation from $\boldsymbol{Y}$ providing full OFDM resolution and unambiguity. Additionally, artifacts due to the transmission pattern should be diminished or eliminated. In order to exploit both range and velocity information appropriately, as previously mentioned, simultaneous reconstruction is required yielding a large-scale two-dimensional problem.

To estimate $\boldsymbol{s}$ in (17), a wide variety of approaches and algorithms exist. Considering the limited real radar hardware, our requirements to the algorithms are efficiency, low complexity, straightforward tuning, fast convergence, reliability, and applicability to large-scale and two-dimensional problems. Considering these requirements, some iterative approaches offer good opportunities, however, for good performance and reliability many iterative algorithms need to be tuned. As shown in [20], perfect tuning of common iterative algorithms is complex and complicated. Furthermore, it is impractical and cumbersome to readjust the algorithms each time the radar scene or signal changes. For this reason, we will only use algorithms that are able to tune themselves and, if necessary, adapt themselves without having to intervene. In the following, three algorithms that meet these condition are presented. Since in their basic implementations none of them is able to straightforwardly solve the large-scale two-dimensional task,

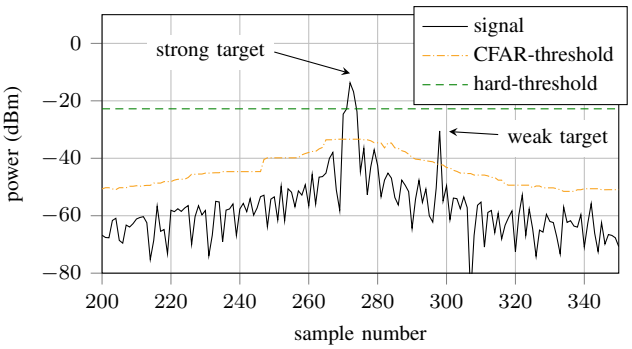

Fig. 5. Comparison of CFAR (-·-·-) and hard-thresholding (- - - -) using a velocity profile comprising two targets (——).

adaptations, generalizations, and enhancements are introduced to their basic structure. We will focus on our adaptations for the algorithms in order to solve the sparse OFDM signal reconstruction in the following. Details on their backgrounds, derivations, and basic implementations can be found in the literature cited.

A. Split Augmented Lagrangian Shrinkage

The split augmented Lagrangian Shrinkage (SALSA) algorithm is presented by [21], [22] as an extension to the augmented direction method of multipliers (ADMM). It is originally intended for image recovery and denoising tasks. Using a regularized version of the Hessian of the fidelity $\boldsymbol{A}^H\boldsymbol{A}$ instead of the gradient information, the algorithm is supposed to solve ℓ_1-minimization problems much faster than related methods.

The iterative procedure can be straightforwardly adjusted to our two-dimensional optimization problem and comes without matrix inversions using only matrix-matrix or matrix-vector operations. A key element is the thresholding step where we apply two-dimensional soft-thresholding. Since the threshold should separate significant signal coefficients from noise, the threshold is derived directly from the noise level estimate of the current signal in every iteration.

B. Hard-Threshold Approximate Message Passing

Approximate Message Passing (AMP) is introduced by [23] as an extension and improvement to iterative thresholding (IT) methods. The two steps of the iteration comprise thresholding and computation of a residual. Originating from IT, AMP is suitable to solve the ℓ_0-minimization problem but does not require any matrix inversion steps. The algorithm can be adjusted to fit the two-dimensional and complex-valued task. The threshold policy in our implementation is hard-thresholding with a fixed number of detections. In every iteration, s elements pass the threshold, where s is proportional or equal to the expected sparsity of the radar scene, which again is equal to the expected number of scatterers. In general, this value is unknown, however, it can be approximated using previous measurements or via estimation based on the disturbed profile.

Compared to IT, the residual is extended by the so-called Onsager correction term. It consists of the measure of indeterminacy and the average of the derivate of the shrinkage/threshold function. It is claimed that by inserting this term, the sparsity undersampling tradeoff is improved such that the theoretical tradeoff for linear programming can be reached with AMP [23]. Furthermore, it guarantees that the noise is approximately Gaussian [24] as well as the linear convergence of $\boldsymbol{s}$. The algorithm is further referred to as hard-threshold AMP (HAMP).

C. Constant False Alarm Rate Approximate Message Passing

A drawback of global soft- and hard-thresholding, as utilized in SALSA and HAMP, is that the same threshold is applied to all elements. However, considering noisy and clutter afflicted radar images, the noise floor is not uniform but depends on the neighboring cells. Using the same threshold for all cells could lead to false alarms due to noise peaks and clutter and therefore high noise and clutter sensitivity. Constant false alarm rate (CFAR) algorithms are designed to consider these effects through estimation of local noise levels for all cells [25]. A choice for the CFAR could be the ordered statistics CFAR (OS-CFAR) that estimates the noise floor based on a neighborhood of p cells and designs a suitable threshold for every cell using a fixed rank. Straightforward parameter adjustment is achieved by deriving the CFAR directly from the CFAR instance used for the usual subsequent target detection. The scaling factor is increased (approximately doubled) and the rank is reduced to 0.5. The number of training cells as well as the neighborhood area shape are identical.

CFAR-thresholding is similar to hard-thresholding except that instead of a global, a local threshold is used for every cell. In Fig. 5, the two threshold policies are depicted using the velocity profile of a scene comprising a strong and a weak target. The global hard-threshold policy only detects the stronger target where the CFAR-threshold, that is better adapted to the signal course, also detects the weaker target.

We therefore propose a third algorithm which is a combination of AMP with OS-CFAR thresholding that will further be referred to as CFAR-AMP. The proposed method is self-tuned since the threshold for every cell is computed based on the estimated local noise. A related application combining AMP and CFAR is the complex AMP (CAMP) algorithm for radar target detection presented in [26].

D. Complexity Consideration

Assuming a range-velocity profile of size $M \times N$ with $10^2 < (M, N) < 10^9$ and w.l.o.g. $N > M$. The number of expected targets s and the size p of the neighborhood in the CFAR are limited to $10^0 < (s, p) < 10^2$.

In each algorithm, a two-dimensional FFT operation along all rows and columns is computed. The complexity of this operation is $\mathcal{O}(MN \log N)$.

The soft-thresholding step in the SALSA algorithm has complexity $\mathcal{O}(MN)$ which is less complex than the FFT. Hence, the complexity of SALSA is $\mathcal{O}(MN \log N)$. The complexity of the hard-thresholding step with fixed detection rate in HAMP depends, besides the matrix size, on the fixed number of expected targets s per iteration. Identifying these s values has complexity $\mathcal{O}(sMN)$ which is larger than the complexity of the FFT and thereby of SALSA. The CFAR-threshold depends, additionally to the matrix size, on p in the noise level estimation step. The complexity of the CFAR-threshold is $\mathcal{O}(MNp \log(p))$ which is also larger than SALSA and, considering the constraints of s and p, comparable to HAMP but slightly worse:

$$\mathcal{O}(\text{SALSA}) < \mathcal{O}(\text{HAMP}) \lessapprox \mathcal{O}(\text{CFAR-AMP}). \tag{18}$$

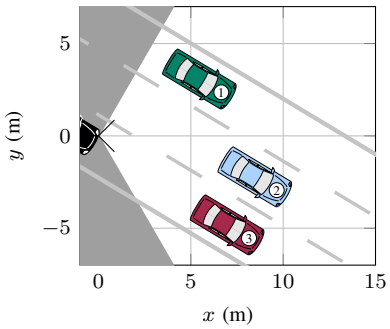

Fig. 6. Sketch of the assumed extended target scene with three moving vehicles.

V. Simulation of Sparse OFDM using Compressed Sensing

In the simulation, additive white Gaussian noise (AWGN) is considered. The reflected energy of every target is computed based on its distance, RCS as well as EIRP (25 dBm) and gain (14 dBi) of the receive antenna. A multilane traffic scene comprising three vehicles is used as depicted in Fig. 6. The relative velocities of the observed vehicles are 0 m/s for vehicle 3 and 15 m/s for vehicle 1 and 2. Additionally, the objects in the scene are modeled as extended targets exhibiting multiple scattering centers using the approach in [27]. Scattering points not directly visible to the radar are neglected which results in ten points in total. The power between the weakest and strongest potential scattering point in the scene is 13 dB.

For tuning of the CS algorithms, we assume that the number of scatterers s is known or an estimate is available. Additionally, it is considered that using an initial underestimate of s, which is increased after every iteration until an overestimation of s is reached, can combat false detections due to signal artifacts and improve the reconstruction. For CFAR-AMP, a neighborhood of $1{\times}20$ cells, a rank of 0.5, and a scaling factor of 20 is used. As stopping criterion, a maximum number of iterations is chosen (SALSA: 20, CFAR-AMP: 10, HAMP: 10).

A. Reconstruction of the Range-Velocity Profile

The resulting range-velocity profiles of the scene for full OFDM as well as sparse OFDM without and with CS are shown in Fig. 7. In Fig. 7a, the result for full OFDM with parameters from Table I is shown.

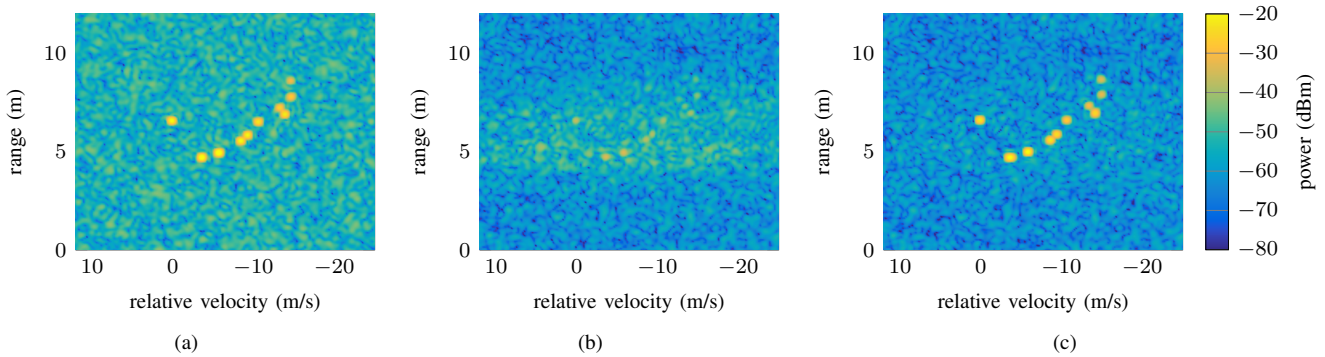

Fig. 7. Evaluation of the range-velocity profile. (a) Full OFDM with baseband bandwidth 1.024 GHz, (b) sparse OFDM using a reduced baseband bandwidth of 127.5 MHz (factor 8) yielding 256 carrier and random number of 2 to 32 symbols per block, and (c) reconstructed profile using CFAR-AMP.

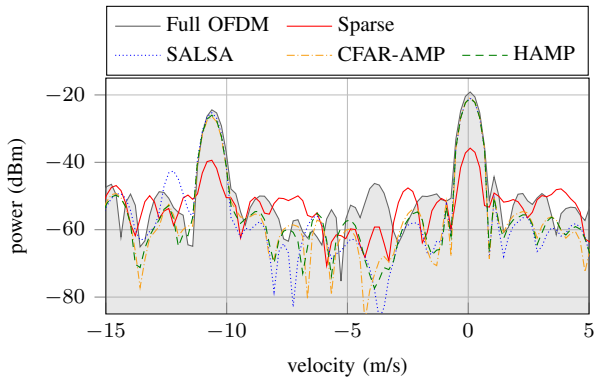

Fig. 8. Constant range cut at $r = 6.6\,\mathrm{m}$ of the full OFDM, sparse OFDM, and reconstructed range-velocity profile using SALSA, CFAR-AMP, and HAMP.

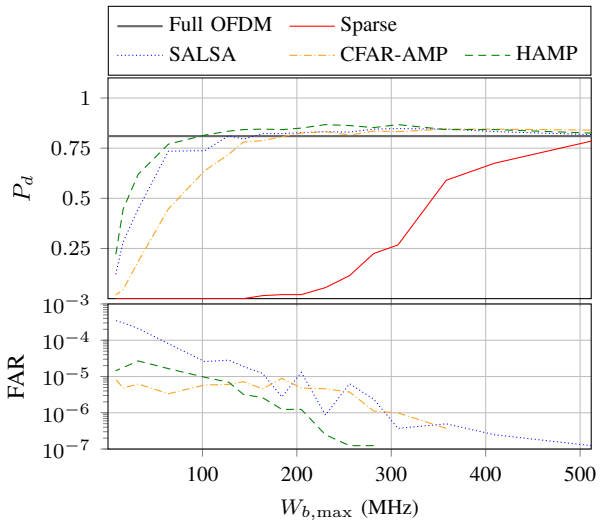

Fig. 9. Comparison of the detection rate (P_d) and false alarm rate (FAR) of full OFDM, sparse OFDM without CS, and reconstructed sparse OFDM using SALSA, CFAR-AMP, and HAMP for different maximum baseband bandwidth ($W_{b,\max}$) and $\mathrm{SNR}_{\min}$ of 15 dB.

For sparse OFDM, 256 subcarriers (=$0.125\mathcal{W}$) are used, yielding a baseband bandwidth of 127.5 MHz, which is a reduction of a factor 8 compared to full OFDM. The block carrier frequency and the number of symbols in every block is chosen randomly, the maximum number is 32 for the latter. In Fig. 7b, the sparse OFDM range-velocity profile before CS is shown. Due to the reduced bandwidth, a drop of the noise level by approximately 9 dB is observable and reflection points disappear between arising artifacts caused by the sparse transmission pattern.

After reconstruction using CFAR-AMP, the profile depicted in Fig. 7c is obtained. The scattering points of the vehicles are clearly visible again and the artifacts due to the sparse transmission have vanished. Furthermore, the noise level is still about 9 dB less compared to full OFDM. This improvement is due to the reduced noise level in sparse OFDM and the peak reconstruction ability of CS that is not affecting the noise level. Hence, in the reconstructed profile, a pseudo-SNR larger than the real SNR can be achieved.

In Fig. 8, the velocity profile at $r = 6.6\,\mathrm{m}$ is shown comprising the results of the full and sparse OFDM as well as the results of all three algorithms. It turns out that using CS, the power levels of the peaks are regained while the noise floor stays decreased. In the sparse profile, target peaks are hardly distinguishable from random noise peaks. After reconstruction, the peaks become sharp again, exhibiting the same peak width as in full OFDM.

B. Detection Probability and False Alarm Rate

Using simulations, the reconstruction ability of the algorithms with respect to different baseband bandwidths and noise impacts are further investigated. The results are evaluated using detection probability (P_d) of the scattering points and the false alarm rate (FAR) in the range-velocity profiles of the full, sparse, and reconstructed signals (using OS-CFAR and a peak search algorithm). The traffic scenario depicted in Fig. 6 is used and the noise impact is controlled using AWGN.

1) P_d and FAR vs. Baseband Bandwidth: The relation between detection rate P_d and FAR and the maximum baseband bandwidth $W_{b,\max}$ is investigated. Sparse OFDM signals with $W_{b,\max}$ from 7.5 MHz to 500 MHz ($0.0078\mathcal{W}$ to $0.5\mathcal{W}$) are simulated. In every OFDM frame, $W_{b,\max}$ is fixed for all blocks and f_b as well as M_b are chosen randomly for every block where $M_{b,\max}$ is 32. In every simulation run, AWGN is applied such that in the comparative full OFDM, the $\mathrm{SNR}_{\min}$ of the weakest scatterer is set fixed to 15 dB. The

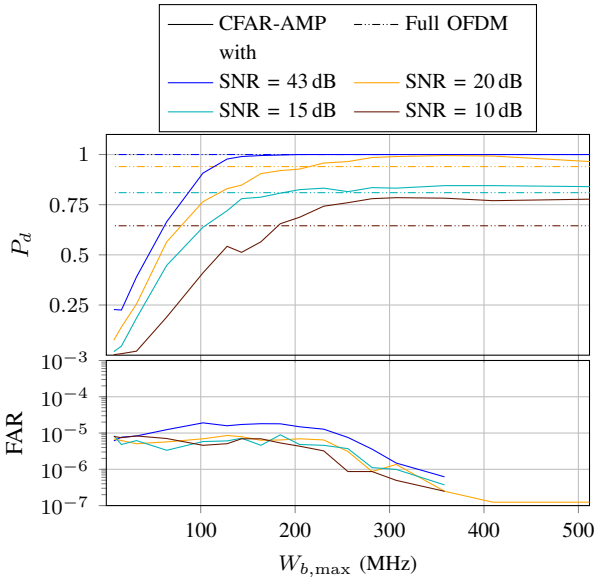

Fig. 10. Comparsion of detection rate (P_d) and false alarm rate (FAR) of full OFDM and sparse OFDM with HAMP reconstruction for different maximum baseband bandwidths ($W_{b,\max}$) at different minimum SNR of 5 dB, 10 dB, 20 dB and 43 dB.

resulting P_d and FAR of the sparse measurement, as well as SALSA, CFAR-AMP, and HAMP reconstruction against $W_{b,\max}$ are shown in Fig. 9. In addition, for comparison, a curve for full OFDM is given (solid line). The P_d of this is 0.81 and the FAR is zero and thus not visible in the graph. As expected, the worst detection probability yields the sparse measurement without CS reconstruction. Using CS, P_d is considerably improved. In comparison to full OFDM, a comparable performance is reached for $W_{b,\max} \geq 100\,\mathrm{MHz}$ using HAMP, and approximately $W_{b,\max} \geq 200\,\mathrm{MHz}$ using CFAR-AMP or SALSA. As a consequence, with the sparse OFDM approach using CS, only 10% to 20% of the baseband and AD/DA conversion bandwidth is needed to achieve similar fidelity as with the full OFDM approach.

Additionally, for 200 MHz to 500 MHz, P_d of the reconstructed signals exceeds the one of full OFDM due to the achievable pseudo-SNR in the CS case. With increasing $W_{b,\max}$, this effect declines and the P_d-curves of the CS algorithms approach the full OFDM P_d.

Looking at the FAR curves, it turns out that with increasing $W_{b,\max}$ the curves decrease, above 350 MHz, no false alarms are registered anymore for HAMP and CFAR-AMP.

2) P_d and FAR vs. SNR: The impact of the noise level, in terms of $\mathrm{SNR_{min}}$, on P_d is shown in Fig. 10 for CFAR-AMP in comparison to full OFDM. It shows that with decreasing $\mathrm{SNR_{min}}$, P_d decreases for every $W_{b,\max}$. Compared to full OFDM, for all configurations an equally good performance is achieved at a baseband bandwidth of at least 200 MHz. For $\mathrm{SNR_{min}} \geq 43\,\mathrm{dB}$, which is a reasonable assumption for OFDM due to the large processing gain of $G_\mathrm{p} = \mathcal{MN}$, even less than 150 MHz baseband bandwidth is sufficient.

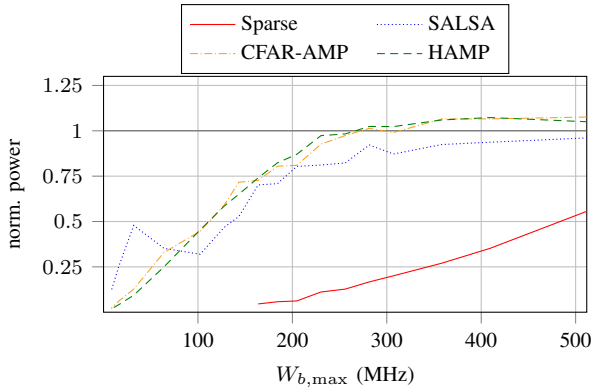

Fig. 11. Achievable relative target power of detected targets in the range-velocity profile with respect to the power of the target in full OFDM.

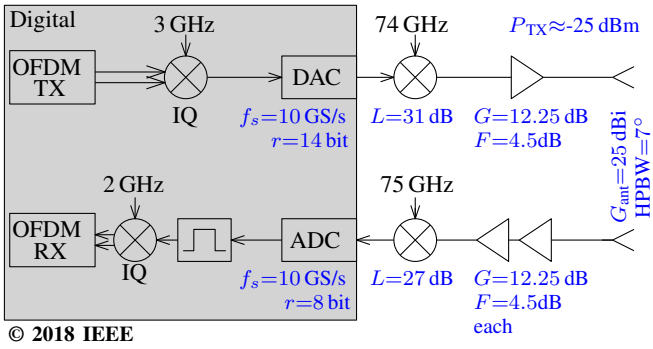

Fig. 12. Schematic of the measurement setup [12].

C. Reconstructed Signal Power

We further investigate the relative reconstructed target power with respect to the expected power in full OFDM against sparse baseband bandwidth. In Fig. 11, the results for $\mathrm{SNR_{min}}$ of 15 dB are presented for different $W_{b,\max}$. The curves of CFAR-AMP and HAMP are similar comprising a linear increase of the relative reconstructed power up to approximately 1 for $W_{b,\max} \leq 250\,\mathrm{MHz}$. The performance may be further increased by using more iterations. The curve for SALSA shows a similar course with small deviation at $W_{b,\max} \leq 100\,\mathrm{MHz}$. For $W_{b,\max} \geq 250\,\mathrm{MHz}$, where the other curves approximated the full OFDM case, the SALSA curve is slightly below the optimum of one.

Fig. 13. Measurement scene comprising a moving vehicle from sensor point of view (left) and the top view of sensor (right).

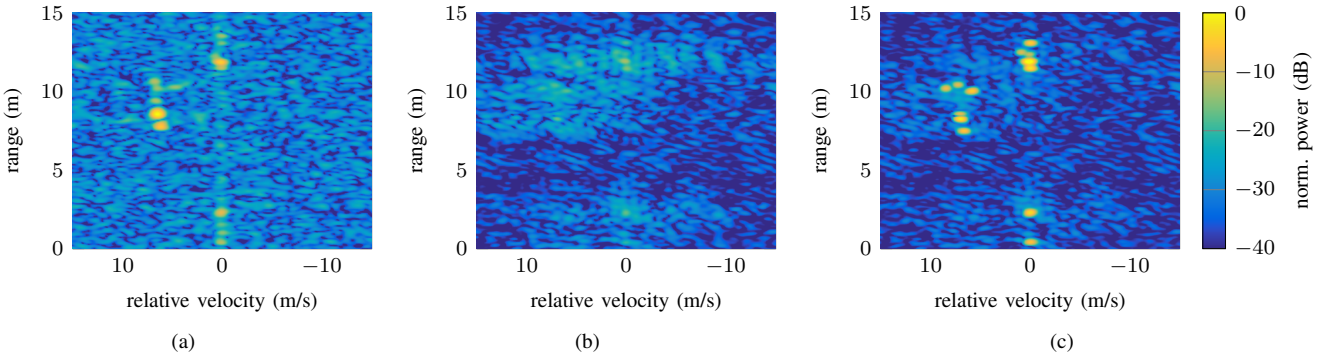

Fig. 14. Range-velocity profiles of the scene in Fig. 13 using full OFDM and sparse OFDM with baseband bandwidths of 1 GHz (2048 subcarriers) and 127.5 MHz (256 subcarriers), respectively. (a) Full OFDM, (b) sparse OFDM without CS, and (c) sparse OFDM with HAMP reconstruction.

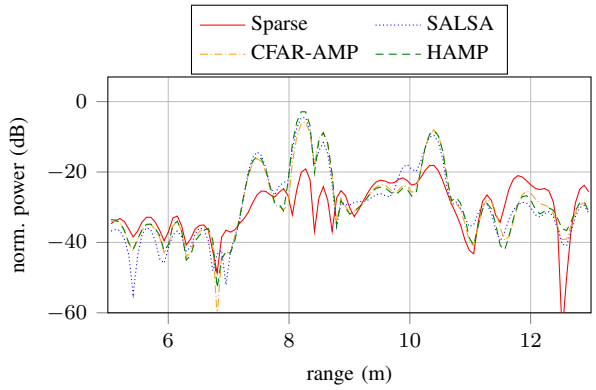

Fig. 15. Constant-velocity cut at $v = 7\,\mathrm{m/s}$ of the sparse OFDM and reconstructed range-velocity profile using SALSA, CFAR-AMP, and HAMP.

VI. Radar Measurement

The results from the simulation are validated using radar measurements. For this purpose, a 77 GHz heterodyne SISO OFDM lab demonstrator is used. The heterodyne setup as shown in Fig. 12 is the same as in [12] and comprises a digital IF stage in the transmit (3 GHz) and receive (2 GHz) path. The up- and down-conversion between baseband and IF frequency is performed in digital domain using single sideband mixers. DA conversion is done by an arbitrary waveform generator (AWG). The analog OFDM transmit signal is then up-converted to 77 GHz using a self-made two-sideband subharmonic mixer at 74 GHz. The received signal is down-converted using a mixer at 75 GHz yielding an IF frequency for the OFDM signal at 2 GHz. The analog signal is sampled with 10 GS/s using an oscilloscope. Digitally, the upper sideband is selected and mixed to baseband using a digital IQ mixer.

The demonstrator allows a maximum baseband bandwidth up to 1 GHz. Thus, it is possible to perform narrowband sparse OFDM measurements as well as wideband full OFDM reference measurements. Due to restrictions of the hardware used in the demonstrator, frequency hopping is performed in the digital domain.

For evaluation, an outdoor traffic scene comprising an approaching vehicle on a street is used. Pictures of the scene from the sensor point of view and of the sensor itself are shown in Fig. 13. The parameters of full OFDM are the same as in Table I. A full OFDM range-velocity profile reference measurement result is depicted in Fig 14a. Some stationary targets and multiple reflections of the moving vehicle are observable. For sparse OFDM, a constant block bandwidth of 127.5 MHz (256 subcarriers) and random block lengths from 2 to 32 symbols are used. The range-velocity profile of a sparse OFDM measurement without CS is shown in Fig. 14b. In the profile, hardly any targets can be recognized. Applying HAMP, the range-velocity profile shown in Fig. 14c is obtained. Multiple moving targets exhibiting a velocity of 5.8 m/s to 8.5 m/s and a range of 7.5 m to 10.5 m become visible. These targets originate from the moving vehicle with high probability. The stationary targets can be assigned to reflections of metal between ground planes, bollards, light posts, and buildings. The noise floor is reduced compared to the full OFDM measurement. Once more, this is a result of the previously mentioned pseudo-SNR.

The range profile at $v = 7\,\mathrm{m/s}$ of the sparse measurement as well as the profiles after reconstruction using SALSA, CFAR-AMP, and HAMP are shown in Fig. 15. All algorithms are able to reconstruct the signal such that all targets become clearly visible.

VII. Conclusion

A sparse OFDM signal processing using compressed sensing techniques is presented which allows OFDM measurements using only a fraction of the required baseband bandwidth of standard OFDM and thereby maintaining resolution and unambiguity of an equivalent wideband signal. Thereby, this method overcomes today's hardware limitations, e.g., AD/DA converter sampling rates or data rates. Combining multiple shorter and narrowband blocks that are transmitted using random carrier frequencies, a channel bandwidth much larger than the instantaneous baseband bandwidth is occupied throughout a single measurement frame. It is shown that, if these blocks are correctly rearranged at the receiver, missing signal parts can be reconstructed using CS methods and a range-velocity profile without resolution and ambiguity loss can be obtained using standard processing based on Fourier transform. Performance and reliability of the proposed method are evaluated using detection probability and false alarm rate. Based on simulations and measurements, it is shown that for

an aimed channel bandwidth of 1 GHz, a baseband bandwidth of approximately 200 MHz is sufficient.

APPENDIX A

Starting from the aimed unknown sparse range-velocity profile $\boldsymbol{R}$, a DFT (row-wise) and IDFT (column-wise) processing yields the corresponding dense time-frequency signal frame $\boldsymbol{Y}'$. In matrix representation, this yields

$$\boldsymbol{Y}' = \boldsymbol{\Psi}^{-1}\boldsymbol{R}\boldsymbol{\Psi} \tag{19}$$

with DFT/IDFT matrices given by $\boldsymbol{\Psi}$ and $\boldsymbol{\Psi}^{-1}$, respectively. However, the dense time-frequency measurement is not available for the sub-Nyquist sampled sparse OFDM case but only its block segments $\boldsymbol{D}_b$ yielding the known measurement frame $\boldsymbol{Y}$. The relation between $\boldsymbol{Y}$ and $\boldsymbol{Y}'$ is given by the transmission pattern $\boldsymbol{P}$ (see (8)) via $\boldsymbol{Y} = \boldsymbol{P} \circ \boldsymbol{Y}'$ where $\boldsymbol{P} \circ \boldsymbol{Y}'$ is the Hadamard product or entrywise product of $\boldsymbol{P}$ and $\boldsymbol{Y}'$. Finally, transferring (17) to sparse OFDM-radar we get

$$\boldsymbol{Y} = \boldsymbol{P} \circ \left(\boldsymbol{\Psi}^{-1}\boldsymbol{R}\boldsymbol{\Psi}\right) + \boldsymbol{N}\,. \tag{20}$$

REFERENCES

[1] T. Hwang, C. Yang, G. Wu, S. Li, and G. Y. Li, "OFDM and Its Wireless Applications: A Survey," *IEEE Trans. on Veh. Technol.*, vol. 58, no. 4, pp. 1673–1694, May 2009.

[2] N. Levanon, "Multifrequency complementary phase-coded radar signal," *IEE Proc. - Radar, Sonar and Navig.*, vol. 147, no. 6, pp. 276–284, 2000.

[3] B. J. Donnet and I. D. Longstaff, "Combining MIMO Radar with OFDM Communications," *Proc. 3rd Eur. Radar Conf*, pp. 37–40, 2006.

[4] D. Garmatyuk, J. Schuerger, and K. Kauffman, "Multifunctional Software-Defined Radar Sensor and Data Communication System," *IEEE Sensors J.*, vol. 11, no. 1, pp. 99–106, Jan. 2011.

[5] C. Sturm and W. Wiesbeck, "Waveform Design and Signal Processing Aspects for Fusion of Wireless Communications and Radar Sensing," *Proc. IEEE*, vol. 99, no. 7, pp. 1236–1259, 2011.

[6] C. R. Berger, B. Demissie, J. Heckenbach, P. Willett, and S. Zhou, "Signal Processing for Passive Radar Using OFDM Waveforms," *IEEE J. Sel. Topics Signal Process.*, vol. 4, no. 1, pp. 226–238, Feb. 2010.

[7] R. F. Tigrek, W. J. A. De Heij, and P. Van Genderen, "Multi-Carrier Radar Waveform Schemes for Range and Doppler Processing," *IEEE Radar Conf.*, pp. 1–5, 2009.

[8] C. Sturm, E. Pancera, T. Zwick, and W. Wiesbeck, "A Novel Approach to OFDM Radar Processing," in *IEEE Radar Conf.*, 2009, pp. 1–4.

[9] G. Lellouch, R. Pribic, and P. van Genderen, "Frequency Agile Stepped OFDM Waveform for HRR," in *Int. Waveform Diversity and Design. Conf.* IEEE, Feb. 2009, pp. 90–93.

[10] G. Lellouch, P. Tran, R. Pribic, and P. Van Genderen, "OFDM waveforms for frequency agility and opportunities for doppler processing radar," *IEEE Radar Conf.*, 2008.

[11] K. Huo, B. Deng, Y. Liu, W. Jiang, and J. Mao, "The Principle of Synthesizing HRRP Based on a New OFDM Phase-coded Stepped-frequency Radar Signal," in *IEEE 10th Int. Conf. Signal Proc.*, Oct. 2010, pp. 1994–1998.

[12] B. Schweizer, C. Knill, D. Schindler, and C. Waldschmidt, "Stepped-Carrier OFDM-Radar Processing Scheme to Retrieve High Resolution Range-Velocity Profile at Low Sampling Rate," *IEEE Trans. Microw. Theory Techn.*, vol. 66, no. 3, pp. 1610–1618, Mar. 2018, to be published.

[13] D. L. Donoho, "Compressed Sensing," *IEEE Trans. Inf. Theory*, vol. 52, no. 4, pp. 1289–1306, 2006.

[14] E. J. Candès, J. K. Romberg, and T. Tao, "Stable Signal Recovery from Incomplete and Inaccurate Measurements," *Comm. Pure Appl. Math.*, vol. 59, no. 8, pp. 1207–1223, Aug. 2006. [Online]. Available: http://doi.wiley.com/10.1002/cpa.20124

[15] C. Berger, S. Zhou, and P. Willett, "Signal Extraction Using Compressed Sensing for Passive Radar with OFDM Signals," in *11th Int. Conf. Inf. Fusion*, 2008, pp. 1–6.

[16] B. Nuss, L. Sit, and T. Zwick, "A Novel Technique for Interference Mitigation in OFDM Radar using Compressed Sensing," in *IEEE MTT-S Int. Conf. Microw. Intell. Mobility*, Mar. 2017, pp. 143–146.

[17] H. Stahl, J. Mietzner, and R. F. H. Fischer, "A Sub-Nyquist Radar System Based on Optimized Sensing Matrices Derived via Sparse Rulers," in *3rd Int. Workshop Compress. Sens. Theory Appl. Radar, Sonar Remote Sens.*, Jun. 2015, pp. 36–40.

[18] G. Lellouch, R. Pribic, and P. Van Genderen, "Merging Frequency Agile OFDM Waveforms and Compressive Sensing into a Novel Radar Concept," in *Eur. Radar Conf.*, Sep. 2009, pp. 137–140.

[19] G. Lellouch, A. K. Mishra, and M. Inggs, "Stepped OFDM Radar Technique to Resolve Range and Doppler Simultaneously," *IEEE Trans. Aerosp. Electron. Syst.*, vol. 51, no. 2, pp. 937–950, Apr. 2015.

[20] A. Maleki and D. L. Donoho, "Optimally Tuned Iterative Reconstruction Algorithms for Compressed Sensing," *IEEE J. Sel. Topics Signal Process.*, vol. 4, no. 2, pp. 330–341, Apr. 2010.

[21] M. A. T. Figueiredo, J. M. Bioucas-Dias, and M. V. Afonso, "Fast frame-based image deconvolution using variable splitting and constrained optimization," in *IEEE/SP 15th Workshop Statistical Signal Process.*, Aug. 2009, pp. 109–112.

[22] M. V. Afonso, J. M. Bioucas-Dias, and M. A. T. Figueiredo, "Fast Image Recovery Using Variable Splitting and Constrained Optimization," *IEEE Trans. Image Process.*, vol. 19, no. 9, pp. 2345–2356, Sep. 2010.

[23] D. L. Donoho, A. Maleki, and A. Montanari, "Message Passing Algorithms for Compressed Sensing," *Proc. Natl. Acad. Sci. USA*, Jul. 2009.

[24] C. A. Metzler, A. Maleki, and R. G. Baraniuk, "From Denoising to Compressed Sensing," *IEEE Trans. Inf. Theory*, vol. 62, no. 9, pp. 5117–5144, Sep. 2016.

[25] H. Rohling, "Radar CFAR Thresholding in Clutter and Multiple Target Situations," *IEEE Trans. Aerosp. Electron. Syst.*, vol. AES-19, no. 4, pp. 608–621, Jul. 1983.

[26] L. Anitori, M. Otten, W. van Rossum, A. Maleki, and R. Baraniuk, "Compressive CFAR Radar Detection," in *IEEE Radar Conf.* IEEE, May 2012, pp. 0320–0325.

[27] M. Bühren and B. Yang, "Automotive Radar Target List Simulation based on Reflection Center Representation of Objects," in *Workshop Intell. Transp.*, Hamburg, Germany, 2006, pp. 161–166.

Christina Knill Christina Knill received the B.Sc. and M.Sc. degree in electrical engineering from Ulm University, Ulm, Germany in 2012 and 2015, respectively. Since 2015, she is pursuing the Ph.D. degree at the Institute of Microwave Engineering, Ulm University, Ulm, Germany.

Her current research interests are OFDM radar signal processing and its application to future adaptive radar sensors for automotive applications.

Benedikt Schweizer Benedikt Schweizer (S'17) received the B.Sc. and the M.Sc. degree in electrical engineering from Ulm University, Ulm, Germany in 2013 and 2016, respectively.

From 2014 to 2015, he was an intern in the integrated circuits group at the Robert Bosch Research and Technology Center in Palo Alto, CA, USA. Since 2016, he is pursuing the Ph.D. degree at the Institute of Microwave Engineering, Ulm University, Ulm, Germany with his main research focus on future digital radar systems.

Susanne Sparrer Susanne Sparrer received the Diploma degree in electrical engineering from Friedrich-Alexander-University Erlangen-Nürnberg, Erlangen, Germany, in 2012. Since 2012, she is pursuing the Ph.D. degree at the Institute of Communications Engineering, Ulm University, Ulm, Germany.

Her current research interests are algorithms for Compressed Sensing, in particular for scenarios in which prior information on the sparse signal is available.

Fabian Roos Fabian Roos (S'15) received the M.Sc. degree from the Karlsruhe Institute of Technology (KIT), formerly Universität Karlsruhe (TH), in 2014. Since September 2014 he is working towards the Ph.D. degree as a Research Assistant at the Institute of Microwave Engineering at Ulm University, Germany. He is interested in automotive radar signal processing, especially for chirp-sequence radar. Currently he is working on adaptivity for chirp-sequence radar.

Robert F.H. Fischer (Senior Member, IEEE) received the Dr.-Ing. degree in 1996, and the habilitation degree in 2001, from the University of Erlangen–Nürnberg, Erlangen, Germany. The subject of his dissertation was multichannel and multicarrier modulation, that of his habilitation was precoding and signal shaping.

Form 1992 to 1996, he was a Research Assistant at the Telecommunications Institute, University of Erlangen–Nürnberg. During 1997, he was with the IBM Research Laboratory, Zürich, Switzerland. In 1998, he returned to the University of Erlangen–Nürnberg, and in 2005 he spent a sabbatical at ETH, Zürich, Switzerland. Since 2011, he has been full professor at the University of Ulm, Germany. Currently, he teaches undergraduate and graduate courses on signals and systems and on digital communications. His research concentrates on fast, reliable, and secure digital transmission including single- and multicarrier modulation techniques; current interests are information theory, coded modulation, digital communications, signal processing, and especially precoding and shaping techniques.

Dr. Fischer received the Dissertation Award form the Technische Fakultät, University of Erlangen–Nürnberg, in 1997, the Publication Award of the German Society of Information Techniques (ITG) in 2000, the Wolfgang Finkelnburg habilitation award in 2002, and the Philipp–Reis–Preis in 2005. He is author of the textbook "Precoding and Signal Shaping for Digital Transmission" (John Wiley & Sons, New York, 2002).

Christian Waldschmidt Christian Waldschmidt (S'01-M'05-SM'13) received the Dipl.Ing. (M.S.E.E.) and Dr.-Ing. (Ph.D.E.E.) degrees from the University of Karlsruhe (TH), Karlsruhe, Germany, in 2001 and 2004, respectively. From 2001 to 2004, he was a Research Assistant with the Institut fr Höchstfrequenztechnik and Elektronik, University of Karlsruhe (TH). Since 2004, he has been with Robert Bosch GmbH, in the business units Corporate Research and Chassis Systems. He was heading different research and development teams in microwave engineering, rf-sensing, and automotive radar.

In 2013, he returned to academia. He was appointed as the Director of the Institute of Microwave Engineering, University Ulm, Germany, as a Full Professor. He has authored or co-authored over 100 scientific publications and over 20 patents. The research topics focus on radar and rf-sensing, mm-wave and submillimeter-wave engineering, antennas and antenna arrays, and rf and array signal processing. He is the Vice Chair of the IEEE MTT-27 Technical Committee (wireless enabled automotive and vehicular applications), the Executive Committee Board Member of the German MTT/AP Joint Chapter, and a member of the ITG Committee Microwave Engineering. In 2015, he served as the TPC Chair of the IEEE Microwave Theory and Techniques Society International Conference on Microwaves for Intelligent Mobility. He is a reviewer for multiple IEEE Transactions and letters.